Adaptive delayed feedback control for stabilizing unstable steady states

Koki Yoshida [1,*] and Keiji Konishi [2,†]

[1]*National Institute of Technology, Toyama College*, 13 Hongo-machi, Toyama City, Toyama 939-8630, Japan
[2]*Graduate School of Engineering, Osaka Metropolitan University*, 1–1 Gakuen-cho, Naka-ku, Sakai, Osaka 599-8531, Japan

Delayed feedback control is a commonly used control method for stabilizing unstable periodic orbits and unstable steady states. The present paper proposes an adaptive tuning delay time rule for delayed feedback control focused on stabilizing unstable steady states. The rule is designed to slowly vary the delay time, increasing the difference between the past and current states of dynamical systems, which induces the delay time to automatically fall into the stability region. We numerically confirm that the tuning rule works well for the Stuart–Landau oscillator, FitzHugh–Nagumo model, and Lorenz system.

I. INTRODUCTION

In the field of nonlinear science, considerable research has been devoted to stabilizing periodic orbits (UPOs) or steady states (USSs) embedded within nonlinear dynamical systems [1]. Delayed feedback control (DFC) [2], one of the most popular methods capable of stabilizing both UPOs [3–11] and USSs [12–20], has garnered attention, since its control law does not rely on information on the desired UPOs or USSs. DFC feeds back a simple signal proportional to the difference between the past (i.e., delayed) and current states of a dynamical system, and can thereby achieve stabilization without complicated calculations. Once DFC successfully achieves the stabilization of a UPO or USS embedded within a system, the stabilized orbit or state can be maintained by a tiny control energy owing to the noninvasiveness of DFC.

To achieve stabilization, the two parameters for DFC, the feedback gain and the delay time, have to be appropriately chosen. Especially, the delay time has to be chosen based on the period of the UPOs or the frequency around the USSs. Thus, the choice of the delay time becomes challenging for real-world situations where exact knowledge of the UPOs or USSs is not available. Furthermore, even after setting an appropriate delay time, stabilization is not maintained in situations where the parameters for the controlled systems shift to other values. To address these challenges, adaptive tuning techniques for the two parameters have been reported as follows: UPOs and USSs can be stabilized by techniques with adaptive feedback gain [21–24]; UPOs can be stabilized by techniques with adaptive delay time [25–31]. However, to the best of the authors' knowledge, there have been few efforts to apply techniques with an adaptive delay time to the stabilization of USSs.[1]

It must be emphasized that, in real applications, such as metal cutting processes [32], combustors [33], direct current

power systems [34], and crowd synchrony on a bridge [35], self-excited periodic oscillations or chaotic oscillations can cause performance degradation or structural damage. For such applications, the stabilization of USSs is a powerful solution to eliminate these harmful oscillatory behaviors. Among the control methods for stabilizing USSs, DFC is one of the most practical methods,[2] since DFC can easily obtain the control signal and also maintain the stabilized state by a tiny control energy owing to its noninvasiveness. However, for some delay times, DFC may induce stabilization of UPOs, which causes a harmful oscillatory behavior in such applications.

The present paper proposes additional functionality to conventional DFC, using a technique with adaptive tuning of the delay time, which enhances the usability and performance of DFC. This technique is focused on stabilizing USSs based on the gradient descent method. The tuning rule is designed such that the delay time varies *sufficiently* slowly to *increase* the difference between the past and current states of dynamical systems. Such an increase induces the delay time to automatically fall into the stability region for conventional DFC. In contrast, the tuning rules aimed at stabilizing UPOs reported in previous studies [25–29] are designed to *decrease* the difference. This contrast means that our tuning rule can avoid the stabilization of UPOs and the consequent harmful oscillatory behavior. Here, we summarize the features of our tuning rule as follows: It is simple and easily implemented, it does not require information about the desired USSs, it can prevent periodic orbits, and it can stabilize some types of USSs that conventional DFC cannot stabilize. These features are useful for real-world situations where oscillatory behavior is harmful and information on the dynamical systems to be stabilized is not available.

The structure of the present paper is as follows. Section II demonstrates limitations in using conventional DFC for stabilizing USSs through some numerical examples. Section III

---

*Contact author: kokiyoshida@nc-toyama.ac.jp

†Contact author: konishi-ees@omu.ac.jp

[1]Subsection V C will discuss the techniques with adaptive delay time [29,30] which have a potential for stabilizing USSs.

[2]Section VI will provide an overview of the control methods for stabilizing USSs, and then clarify the relationship between them and our proposal.

proposes the adaptive tuning rule and numerically confirms its performance on linear systems. Section IV applies the adaptive tuning rule to the Stuart–Landau oscillator, the normal form of Hopf bifurcation. Section V numerically confirms the effectiveness of the adaptive tuning rule for other popular oscillators, the FitzHugh–Nagumo model and the Lorenz system, and discusses the relation to previous studies dealing with adaptive tuning of the delay time. Section VI overviews several control methods for stabilizing USSs with noninvasive properties. Section VII concludes our results.

II. LIMITATIONS IN USING DFC

This section outlines limitations in using DFC. We consider a Stuart–Landau (SL) oscillator with conventional DFC, as used in Ref. [36],

$$\dot{z}(t) = [\lambda + i\omega - (1 + ib)|z(t)|^2]z(t) - k[z(t) - z(t - \tau)], \quad (1)$$

where $z(t) = x(t) + iy(t)$ is a complex state variable at time $t \in \mathbb{R}$. The real parameters, $\lambda > 0$ and $\omega > 0$, correspond to the damping and intrinsic frequency near the steady state $(x, y) = (0, 0)$, respectively. The parameter $b \in \mathbb{R}$ represents the frequency dependency on the oscillator amplitude. The SL oscillator without control (i.e., $k = 0$ or $\tau = 0$) has an unstable steady state and a stable limit cycle with amplitude $\sqrt{\lambda}$ and frequency $\omega - b\lambda$. The conventional controller used in Eq. (1) has two parameters: feedback gain $k \in \mathbb{R}$ and delay time $\tau \geqslant 0$.

Figure 1(a) shows the time series of $x(t) = \text{Re}[z(t)]$ for $\lambda = 1, \omega = \pi, b = 0.8\pi$, and $k = 0.6$, for two different delay times, $\tau = 1.0$ (broken black line) and $\tau = 1.3$ (solid gray line). System (1) without control runs for $t \in [0, 20)$ with the initial state $(x(0), y(0)) = (1, 0)$. After that, DFC starts to work at $t = 20$ with the initial function which is the trajectory of system (1) without control for $t \in [20 - \tau, 20)$. Throughout this paper, we use such initial functions (see our previous study [37] and references therein for more details) and the MATLAB function ddesd for all numerical simulations. As can be seen, the state variable does not converge to the steady state (i.e., stabilization fails) for both $\tau = 1.0$ and 1.3. Note that, the steady state is analytically guaranteed to be locally stable for $\tau = 1.0$ and locally unstable for $\tau = 1.3$. Hence, for $\tau = 1.3$, the behavior of the state variable agrees with the stability. In contrast, for $\tau = 1.0$, the state variable fails to converge to the *stable* steady state because the initial state is not within its basin. A well-known major limitation when using DFC is that the local dynamics of the steady state (i.e., the Jacobian matrix) is required when designing τ to obtain a locally stable steady state. The above numerical examples indicate another limitation: Stabilization fails even with a *stable* steady state.

To avoid these limitations, the present study proposes applying adaptive tuning of the delay time in DFC,

$$\dot{\tau}(t) = -\beta \tanh g(t), \quad (2a)$$

$$\dot{u}(t) = \gamma\{z(t - \tau) - u(t)\}, \quad (2b)$$

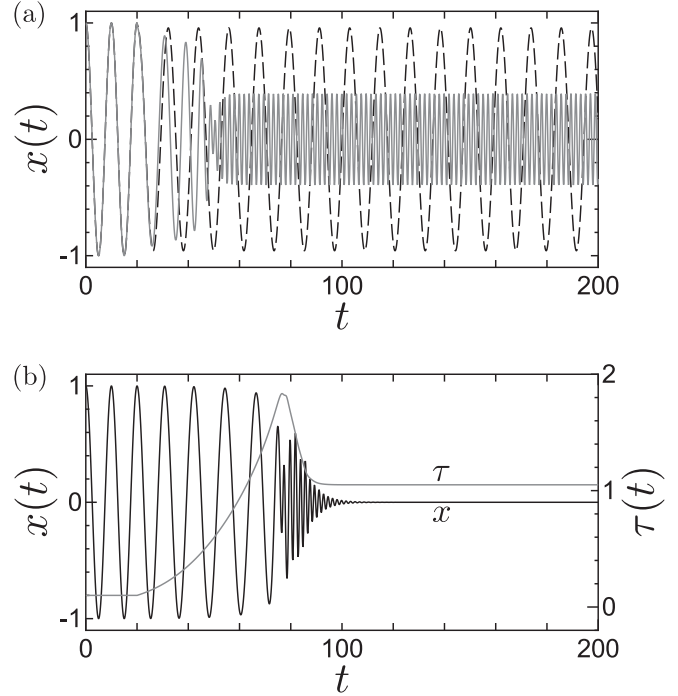$$g(t) := -h(z(t) - z(t - \tau), \gamma\{z(t - \tau) - u(t)\}), \quad (2c)$$

FIG. 1. Time series of real part $x(t)$ of state variable $z(t)$ in a Stuart–Landau oscillator with (a) conventional DFC (1) and (b) adaptive tuning (2). The parameters are set to $\lambda = 1, \omega = \pi, b = 0.8\pi$, and $k = 0.6$. Control starts at $t = 20$. In panel (a), two different delay times, $\tau = 1.0$ (broken black line) and $\tau = 1.3$ (solid gray line), are used. In panel (b), the time series of the delay time $\tau(t)$ with initial value $\tau(0) = 0.1$ for $\beta = 0.1$ and $\gamma = 100$ is also plotted.

where $u(t) \in \mathbb{C}$ is an additional state and the function h is defined by

$$h(z_1, z_2) := z_1\bar{z}_2 + \bar{z}_1 z_2, \quad (3)$$

for $z_{1,2} \in \mathbb{C}$. Here, the parameter $\beta > 0$ and the parameter $\gamma > 0$ are set to a small value and a large value, respectively. The background to how we obtain Eq. (2) will be explained in the next section. Figure 1(b) shows the time series of $x(t) = \text{Re}[z(t)]$ and delay time $\tau(t)$ in system (1) with adaptive tuning (2) applied with $\beta = 0.1$ and $\gamma = 100$. The parameters and the initial condition are the same as those in Fig. 1(a). The initial delay time is set to $\tau(0) = 0.1$ and DFC with adaptive tuning (2) starts at $t = 20$. It can be seen that $\tau(t)$ slowly increases to $\tau(76.6) = 1.83$. As a result, the amplitude and frequency of the oscillating $x(t)$ decreases and increases, respectively. Eventually, $\tau(t)$ decreases and then converges to 1.05, and $x(t)$ successfully reaches the steady state.

III. ADAPTIVE TUNING OF DELAY TIME

This section details the concept and tuning rule (2) used in the preceding section.

A. Stability boundaries of delay time [15,16]

It is clear that the stability of the steady state in system (1) with adaptive tuning (2) cannot be analyzed using
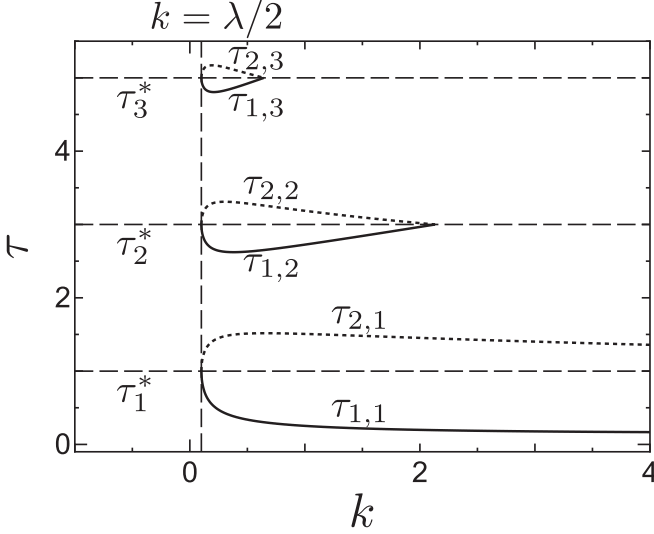
FIG. 2. Stability regions bounded by curves (7) for $\lambda = 0.2$ and $\omega = \pi$ in the k–τ plane. The solid and dotted lines represent $\tau_{1,n}$ and $\tau_{2,n}$, respectively. The regions are given by $\tau \in (\tau_{1,n}, \tau_{2,n})$. The broken lines represent τ_n^* satisfying Eq. (6) and $k = \lambda/2$.

FIG. 3. Behavior of state variable $z(t) = x(t) + \mathrm{i}y(t)$ of system (4) for fixed $\tau = 1.6$ with $\lambda = 0.2$, $\omega = \pi$, and $k = 0.2$: The open circle represents the unstable focus $(x, y) = (0, 0)$. The three dots indicate $z(t)$, $z(t - \tau)$ with $\tau = 1.6$, and $z(t - \tau_1^*)$ with $\tau_1^* = 1$.

characteristic functions, since the dynamics of the steady state depends on the state-dependent time delay. However, for small values of β, the delay time $\tau(t)$ in the tuning rule (2) varies quite slowly compared to the intrinsic frequency of USSs. Thus, although we cannot provide a rigorous analysis of the stability, it is reasonable to consider that understanding the behavior of dynamical systems under conventional DFC (i.e., $\beta = 0$) around USSs is helpful for evaluating systems under DFC having a tuning rule (2) with small β.

Now, let us briefly review the stability boundaries of the delay time for conventional DFC [15,16]. We consider an unstable focus near the Hopf bifurcation point. The linear dynamics around the focus with conventional DFC can be described by

$$\dot{z}(t) = (\lambda + \mathrm{i}\omega)z(t) - k[z(t) - z(t - \tau)]. \tag{4}$$

The stability of system (4) is governed by the characteristic equation,

$$\Lambda + k(1 - e^{-\Lambda\tau}) - (\lambda + \mathrm{i}\omega) = 0. \tag{5}$$

The rightmost root of Eq. (5) has a minimum real part if the delay time is set to [16]

$$\tau = \tau_n^* = (2n - 1)\pi/\omega, \quad n = 1, 2, 3, \ldots. \tag{6}$$

The stability boundaries of τ for $k > \lambda/2$ [15] are given by

$$\tau_{1,n} = \frac{2(n-1)\pi + \arccos\left(\frac{k-\lambda}{k}\right)}{\omega - \sqrt{(2k-\lambda)\lambda}}, \tag{7a}$$

$$\tau_{2,n} = \frac{2n\pi - \arccos\left(\frac{k-\lambda}{k}\right)}{\omega + \sqrt{(2k-\lambda)\lambda}}, \tag{7b}$$

for $n = 1, 2, 3, \ldots$.

The boundaries (7) for $\lambda = 0.2$ and $\omega = \pi$ in the k–τ plane are plotted in Fig. 2. The solid and dotted lines represent $\tau_{1,n}$ and $\tau_{2,n}$, respectively. For k satisfying $\tau_{1,n} < \tau_{2,n}$, system (4)
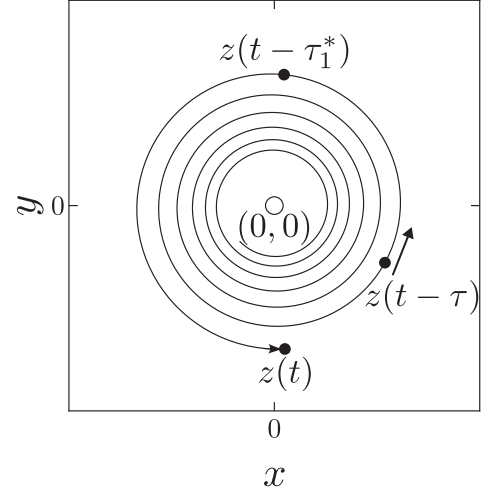
is stable if and only if $\tau \in (\tau_{1,n}, \tau_{2,n})$ holds. The broken lines represent τ satisfying Eq. (6) and $k = \lambda/2$.

B. Concept of adaptive tuning

As mentioned in Sec. II, a limitation with DFC is that an appropriate value τ for inducing stability cannot be designed if ω or λ is unknown [see Eq. (7)]. To avoid this limitation, the present study adds an adaptive function, which automatically tunes $\tau(t)$ slowly, to the controller. An intuitive concept of this tuning is that $\tau(t)$ automatically moves inside the stability regions $(\tau_{1,n}, \tau_{2,n})$ at a slow pace. We note that this concept can be implemented if $\tau(t)$ behaves as $\dot{\tau}(t) > 0$ below $\tau_{1,n}$ and as $\dot{\tau}(t) < 0$ above $\tau_{2,n}$.

It is obvious that, for τ slightly below $\tau_{1,n}$ or above $\tau_{2,n}$, Eq. (5) has an unstable complex root near the imaginary axis. As $\tau(t)$ moves slowly, for such τ, after a sufficiently long time has passed, the state variable behaves as for conventional DFC, which can be expressed by $z(t) \sim \exp[(p + \mathrm{i}q)t]$, where p and q represent the damping and the frequency of the unstable rightmost root Λ, respectively, and the symbol $\sim$ denotes that the left-hand side of the equation is proportional to the right-hand side. The behavior for fixed $\tau = 1.6$ with $\lambda = 0.2$, $\omega = \pi$, and $k = 0.2$ is illustrated in the x–y plane in Fig. 3. The state $z(t)$ moves spirally outward from the unstable focus $(0,0)$ represented by the open circle, with frequency q. The three dots in Fig. 3 represent the current state $z(t)$, the past state $z(t - \tau)$ with $\tau = 1.6 > \tau_{2,1}$, and the past state $z(t - \tau_1^*)$ with $\tau_1^* = 1$. To stabilize the focus, τ must decrease from 1.6 and satisfy $\tau \in (\tau_{1,1}, \tau_{2,1})$ with $\tau_{1,1} = 0.534$ and $\tau_{2,1} = 1.410$. This corresponds to the fact that $z(t - \tau)$ moves away from $z(t)$ in the direction of the arrow on the phase plane in Fig. 3. It can be expected that $z(t)$ will converges to $(0,0)$ when τ reaches τ_1^*, because the control signal $-k[z(t) - z(t - \tau)]$ acts to pull $z(t)$ to $(0,0)$. Based on this concept and the

well-known gradient descent method, we provide the details of the adaptive tuning below.

C. Control law for adaptive tuning

We introduce a negative scalar-valued function based on the difference between $z(t)$ and $z(t - \tau)$,

$$\Delta(t, \tau) := -|z(t) - z(t - \tau)|^2 \leqslant 0, \qquad (8)$$

which becomes zero when $z(t - \tau) = z(t)$ holds. Note that $\Delta(t, \tau)$ decreases with increasing difference between $z(t)$ and $z(t - \tau)$. In the case of Fig. 3, if τ approaches τ_1^*, then $\Delta(t, \tau)$ becomes smaller[3] compared to $\Delta(t, 1.6)$. To realize the adaptive tuning concept, $\tau(t)$ based on the gradient descent method should be tuned by

$$\dot{\tau}(t) = -\beta \frac{d\Delta(t, \tau)}{d\tau}. \qquad (9)$$

Obviously, it is not easy to numerically implement the right-hand side of Eq. (9) because, in practical situations, the derivative signal of $\Delta(t, \tau)$ has to be produced from noisy measurements of $z(t)$. Such a derivation with noise induces large undesirable high-frequency fluctuations of $\dot{\tau}(t)$. To avoid such fluctuations, we use two approximations. The first approximation, under the assumption that $\tau(t)$ moves sufficiently slow, is as follows:

$$\frac{d\Delta(t, \tau)}{d\tau} = -h\left(z(t) - z(t - \tau), \frac{d}{d\tau}[-z(t - \tau)]\right),$$

$$\approx -h(z(t) - z(t - \tau), \dot{z}(t - \tau)), \qquad (10)$$

where the symbol $\approx$ denotes an approximation between the left- and right-hand sides of equation. The time derivative $\dot{z}(t - \tau)$ in Eq. (10) is still weak against noise. Thus, we employ the second approximation as follows: the time derivative can be estimated via a low-pass filter (2b), $\dot{z}(t - \tau) \approx \gamma[z(t - \tau) - u(t)]$, where the cutoff frequency parameter γ should be sufficiently large for $z(t - \tau) - u(t)$ to be close to $\dot{z}(t - \tau)$ (see Ref. [28]). As a result, adaptive tuning (2) requires only the current state $z(t)$ and the past state $z(t - \tau)$, which can be easily measured. In addition to the approximations, for $\tau(t)$ to be varied slowly, the hyperbolic tangent function is used to restrict $g(t)$ within $(-1, +1)$ and the parameter $\beta > 0$, which determines the variation rate of $\tanh g(t)$, is chosen to be sufficiently small. In summary, adaptive tuning (2) is derived from ideal tuning based on the gradient descent method (9) with the mentioned approximations and restriction.

The main purpose of the present paper is to show that adaptive tuning (2) works well for various dynamical systems without requiring knowledge of USSs. The effectiveness of the method is demonstrated by the results of numerical simulations provided in Secs. IV and V. Unfortunately, it is quite difficult to *analytically* prove that adaptive tuning (2)

works well because it is governed by dynamical equations that include two factors, the nonlinearity and the state-dependent delay time in Eq. (2). Despite this difficulty, in the neighborhood of USSs with the assumption of small β, we can show that the behavior of $\tau(t)$ in a linear system (4) with adaptive tuning (2) exhibits the following properties (see Appendix A for more details).

Property 1. $\tau(t)$ slightly below $\tau_{1,n}$ or slightly above $\tau_{2,n}$ moves inside of the stability regions due to $\dot{\tau}(t) > 0$ or $\dot{\tau}(t) < 0$, respectively.

Property 2. Once $\tau(t)$ falls into the stability region, the stabilization is achieved with $\dot{\tau}(t) \to 0$ as $t \to +\infty$.

Note that Property 1 describes the behavior of $\tau(t)$ only near the stability boundaries. The next subsection numerically supports these properties and shows that adaptive tuning (2) works well even for an initial $\tau(0)$ far from the boundaries.
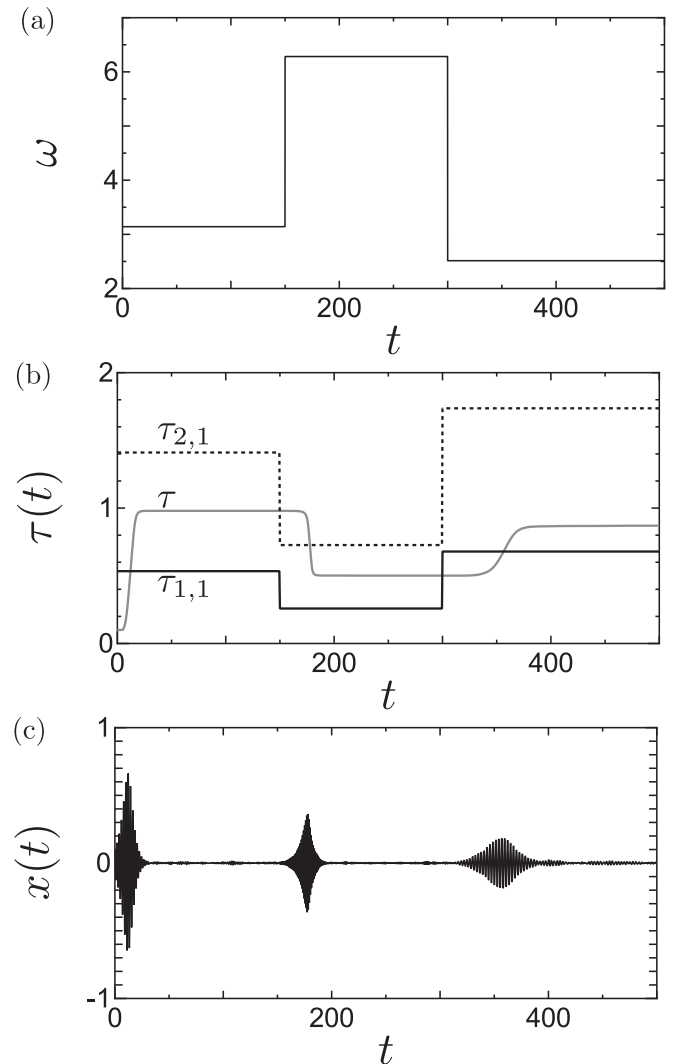

FIG. 4. Behavior of linear system (4) with adaptive tuning (2): (a) $\omega \in \{\pi, 2\pi, 0.8\pi\}$, (b) $\tau_{1,1}, \tau_{2,1}, \tau(t)$, and (c) $x(t) = \text{Re}[z(t)]$. The parameters are fixed as $\lambda = 0.2, k = 0.2, \beta = 0.1$, and $\gamma = 100$. The initial delay time is set to $\tau(0) = 0.1$, and DFC with adaptive tuning starts at $t = 5$.

---

[3]It should be noted that, if the ideal situation, $p = 0$ and $q = \omega$, always holds, $\Delta(t, \tau)$ takes a minimum value at τ_1^*. However, in general, this situation does not hold, as in Fig. 3, where $\Delta(t, \tau)$ takes a minimum value at $\tau = 0.94$, only slightly different from $\tau_1^* = 1$.

D. Numerical test for linear systems

Let us numerically confirm the performance of adaptive tuning (2) for linear system (4). To confirm that Properties 1 and 2 are satisfied and adaptive tuning (2) works well even for the initial τ far from the boundaries, we fix the parameters $\lambda = 0.2$, $k = 0.2$, $\beta = 0.1$, and $\gamma = 100$, while ω shifts to the three values, π, 2π, and 0.8π, at long intervals as shown in Fig. 4(a). Gaussian noise with zero mean and a variance of 0.0001 is applied to both the real and imaginary parts of the right-hand side of Eq. (4). The initial values are set to $(z(0), u(0), \tau(0)) = (0.1, 0, 0.1)$, and DFC with adaptive tuning starts at $t = 5$. Figure 4(b) illustrates the time series of $\tau(t)$ and the stability boundaries (7) for the three values of ω. Note that $\tau(0)$ is set to a value slightly above 0. Since $\Delta(t, \tau)$ takes its maximum value of 0 at $\tau = 0$, a decrease in $\Delta(t, \tau)$ corresponds to an increase in $\tau(t)$, for which $\tau(t)$ approaches the stability boundary $\tau_{1,1}$. The time series of $x(t)$ is shown in Fig. 4(c). For $t \in [0, 12]$, the amplitude of $x(t)$ increases because $\tau(t) \notin (\tau_{1,1}, \tau_{2,1})$. For $t \in [5, 25]$, $\tau(t)$ increases and then moves inside the stability region $(\tau_{1,1}, \tau_{2,1})$. For $t \in [25, 150]$, $\tau(t)$ remains within the region and thus $x(t)$ converges to zero. At $t = 150$, as ω shifts to 2π, $\tau(t)$ jumps out of the stability region. For $t \in [150, 300]$, the adaptive tuning takes $\tau(t)$, which is far from the boundaries for $\omega = 2\pi$ at $t = 150$, into the stability region, and $\tau(t)$ automatically stops changing after achieving stabilization. Similar phenomena also occur for $t \in [300, 500]$ for $\omega = 0.8\pi$. These numerical results support the two properties and the performance of adaptive tuning (2) for $\tau(t)$ far from the boundaries.

IV. STABILIZATION OF SL OSCILLATOR

Let us apply adaptive tuning (2) to the Stuart–Landau oscillator, the normal form of Hopf bifurcation. The dynamics of SL oscillator (1) with adaptive tuning (2) is described by the polar coordinate expression of complex numbers, $z(t) = r(t)e^{i\theta(t)}$:

$$\dot{r}(t) = \lambda r(t) - r^3(t) - k(r(t)$$
$$-r[t - \tau(t)] \cos\{\theta[t - \tau(t)] - \theta(t)\}), \quad (11a)$$

$$\dot{\theta}(t) = \omega - br^2(t)$$
$$+k\left(\frac{r[t - \tau(t)]}{r(t)} \sin\{\theta[t - \tau(t)] - \theta(t)\}\right). \quad (11b)$$

If τ is fixed, then a limit cycle exists with amplitude $r^* = r(t) = r(t - \tau)$ and frequency $\Omega = \{\theta(t) - \theta(t - \tau)\}/\tau$, which satisfy $\dot{r}(t) = 0$ and $\dot{\theta}(t) = \Omega$. We set the parameters to $\lambda = 1$, $\omega = \pi$, $k = 0.6$, $\beta = 0.1$, and $\gamma = 100$. Note that the stability region for the steady state, which is determined by Eq. (7), is given by

$$\tau \in (\tau_{1,1}, \tau_{2,1}) = (0.8538, 1.1097). \quad (12)$$

Now we show the behavior of SL oscillator (11) with adaptive tuning (2) for three cases, $b = 0$, $b < 0$, and $b > 0$.

For $b = 0$, the frequency of SL oscillator (11) without control (i.e., $k = 0$ or $\tau = 0$) is independent of its amplitude and the oscillator has a stable limit cycle with period 2. The trajectory of SL oscillator (11) with adaptive tuning (2) in the τ–r phase plane is shown in Fig. 5(a), where the initial amplitude $r(0) = 1$ is fixed and the three initial delays
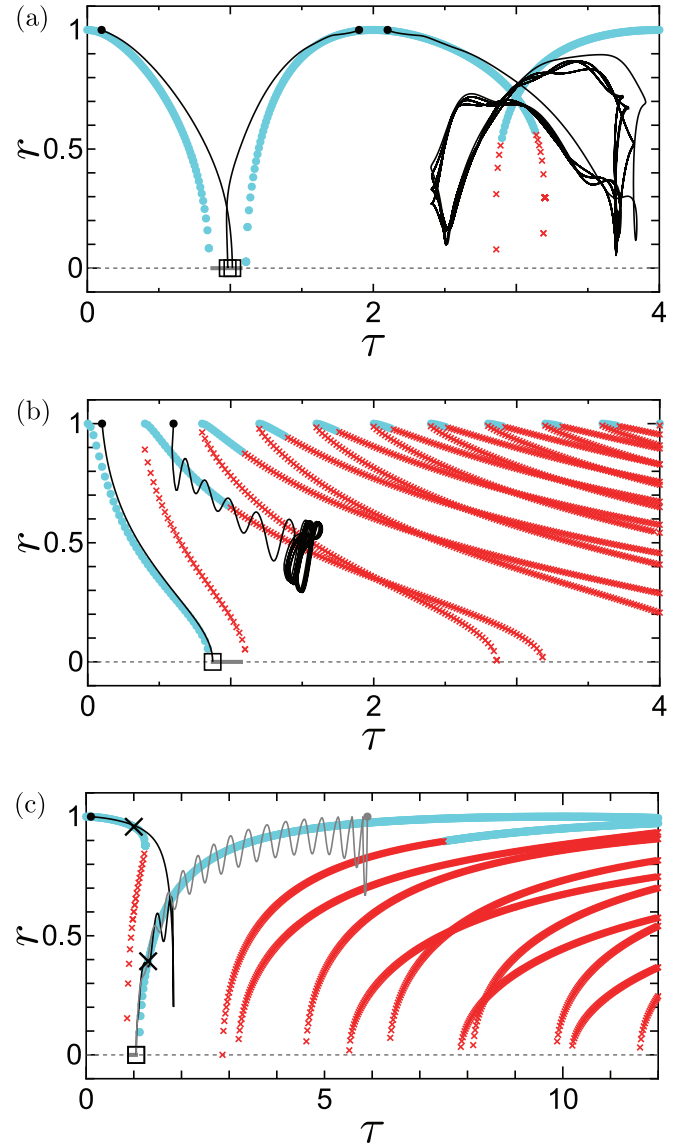

FIG. 5. Trajectories of Stuart–Landau oscillator (11) with adaptive tuning (2) for (a) $b = 0$, (b) $b = -4\pi$, and (c) $b = 0.8\pi$. The parameters are set to $\lambda = 1$, $\omega = \pi$, $k = 0.6$, $\beta = 0.1$, and $\gamma = 100$. The black [and gray in panel (c)] dots, the solid lines, and the squares represent the initial states, the trajectories, and convergence point on the steady state, respectively. The stable and unstable steady states at $r = 0$ are described by the gray solid and dotted lines, respectively. The stable and unstable r^* without tuning are plotted by the cyan (light gray) dots and red (black) crosses. The two big black crosses in panel (c) correspond to Fig. 1(a).

$\tau(0) = 0.1$, 1.9, and 2.1 represented by the three black dots are used. DFC and the tuning start at time $t = 20$. The trajectory for each $\tau(0)$ is plotted by a solid black line. The amplitude r^* of the periodic solutions for SL oscillator (11) without adaptive tuning (2) (i.e., with only the conventional DFC) are plotted. The cyan (light gray) dots and red (black) crosses represent stable and unstable r^*. The solid and dotted gray lines indicate the stable and unstable steady states $r^* = 0$. *Supercritical* Hopf bifurcation occurs at both $\tau = \tau_{1,1}$ and $\tau = \tau_{2,1}$. We note that, if $\tau(t)$ varies very slowly, the trajectory should move along a stable r^*. As can be seen in Fig. 5(a), the

trajectories with $\tau(0) = 0.1$ and 1.9, where $\tau(0)$ are smaller than the period 2 of the stable limit cycle in oscillator (11) without control, follow the downward curve for the stable r^*, and then eventually fall within the stability region (12), where the trajectories remain at $r^* = 0$. The square represents the steady state where the trajectory converges. In contrast, while the trajectory with $\tau(0) = 2.1$ greater than the period 2, also follows the stable r^*, it does not converge on $r^* = 0$ because r^* turns unstable and no stability region exists around $\tau = 3$. As a result, the trajectory alternates between following r^* and jumping to r^*, and thus the stabilization fails for $\tau(0) = 2.1$.

For $b < 0$, the frequency of SL oscillator (11) without control increases with an increase in its amplitude. Figure 5(b) shows the trajectory and r^* for $b = -4\pi$, where SL oscillator (11) without control has a stable limit cycle with period 0.4. The stability of $r^* = 0$ is equivalent to that for $b = 0$; however, $r^* > 0$ and its stability for $b < 0$ is different from that for $b = 0$. The *supercritical (subcritical)* Hopf bifurcation occurs at $\tau = \tau_{1,1}$ ($\tau = \tau_{2,1}$). The trajectory with $\tau(0) = 0.1$, which is smaller than the period 0.4, follows the downward curve for the stable r^*, and then falls within the stability region. In contrast, the trajectory with $\tau(0) = 0.6$, which is greater than the period 0.4, tracks down only for a period because r^* turns unstable.

For $b > 0$, the frequency of SL oscillator (11) without control decreases with an increase in its amplitude. Figure 5(c) shows the trajectory and r^* for $b = 0.8\pi$, where SL oscillator (11) without control has a stable limit cycle with period 10. The stability of $r^* = 0$ is equivalent to that for $b = 0$ and $b = -4\pi$; however, $r^* > 0$ and its stability for $b > 0$ is different from that for $b = 0$ and $b = -4\pi$. Note that the two big black crosses in Fig. 5(c), where stable limit cycles occur in oscillator (11), correspond to the time series of Fig. 1(a). The *subcritical (supercritical)* Hopf bifurcation occurs at $\tau = \tau_{1,1}$ ($\tau = \tau_{2,1}$). The trajectory with $\tau(0) = 0.1$ consists of the following three processes: (i) The trajectory starts from $\tau(0) = 0.1$ and follows the stable r^* downwards; (ii) The trajectory jumps down to the other stable r^*; (iii) The trajectory follows the other stable r^* downwards and then falls within the stability region. Process (ii) occurs because the stable r^* in process (i) disappears due to the saddle-node bifurcation. Note that the time series of $\tau(t)$ in Fig. 1(b) corresponds to the trajectory (i.e., solid black line) of Fig. 5(c). The behavior of $\tau(t)$ in Fig. 1(b) can be explained by these three processes: For process (i), $\tau(t)$ increases from $\tau(0) = 0.1$; For process (ii), the trend of $\tau(t)$ changes from an increase to a decrease; For process (iii), $\tau(t)$ decreases to 1.05. In addition, the trajectory with $\tau(0) = 5.9$ is plotted by the gray solid line. It can be observed that $\tau(t)$ follows the stable r^*, which leads to stabilization.

The numerical results in Fig. 5 reveal that the stabilization depends on the structure of r^*, the type of bifurcation, and the initial delay $\tau(0)$. Furthermore, for all $b \in \{0, -4\pi, 0.8\pi\}$, we see that the stabilization is achieved when $\tau(0)$ is smaller than the period of the stable limit cycle without control. We have numerically confirmed that the stabilization occurs for any $\tau(0)$ smaller than the period (see Appendix B). In contrast, the stabilization fails in some cases when $\tau(0)$ is greater than the period. This implies that for small $\tau(0)$, the tuning induces stability independently of b.
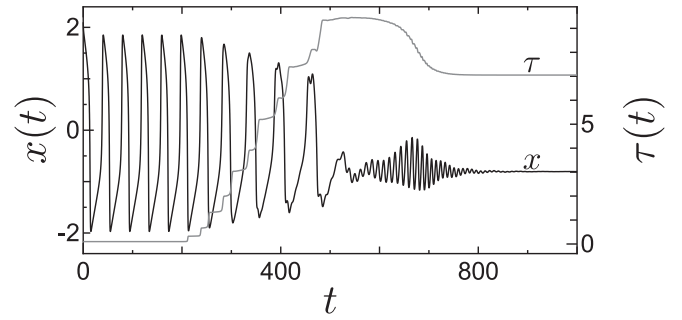

FIG. 6. Time series of state variable $x(t)$ and delay time $\tau(t)$ in FHN model (13) with adaptive tuning (2) for $k = 0.5$, $\beta = 0.25$, and $\gamma = 100$.

V. OTHER OSCILLATORS

This section numerically confirms that adaptive tuning (2) works well for two other commonly used oscillators, the FitzHugh–Nagumo model [38,39] and the Lorenz system [40]. In addition, we discuss two previous studies [29,30] and compare the control performance of tuning rule (2) to that of the previous studies.

A. FitzHugh–Nagumo model

In the FitzHugh–Nagumo (FHN) model, the oscillation frequency of the limit cycles is highly dependent on the amplitude. The FHN model with DFC is described by

$$\dot{x}(t) = x(t) - \tfrac{1}{3}x^3(t) - y(t) + 0.5 - k\{x(t) - x[t - \tau(t)]\},$$
(13a)

$$\dot{y}(t) = 0.08[x(t) + 0.7 - 0.8y(t)],$$
(13b)

where $x(t) \in \mathbb{R}$ and $y(t) \in \mathbb{R}$ are the state variables. The FHN model (13) without control has an unstable steady state $(x, y) = (-0.8048, -0.1311)$ and a stable limit cycle with a period of 39.5. Note that, for real situations, it is reasonable to restrict the applicable variables for feedback. Thus, we suppose that DFC with $k = 0.5$ only uses the variable x, while adaptive tuning (2) uses $x(t)$ instead of $z(t)$. The parameters for tuning rule (2) are set to $\beta = 0.25$ and $\gamma = 100$. Figure 6 shows the time series of $x(t)$ and $\tau(t)$ from the initial states $(x(0), y(0), u(0), \tau(0)) = (2.1, 0, 0, 0.1)$, where DFC with adaptive tuning (2) starts at $t = 200$. We observe that the adaptive tuning can induce stabilization even with a single variable, $x(t)$.

We now investigate the influence of the initial delay $\tau(0) \in [0.1, 100]$ on the performance of adaptive tuning (2). The parameters and other initial conditions are the same as for Fig. 6. The amplitudes of $x(t)$ and the delay $\tau(t)$ at $t = 3000$ are plotted against $\tau(0) \in [0.1, 100]$ in Fig. 7. The solid gray line represents the amplitudes of $x(t)$ for $t \in [2900, 3000]$.[4] The solid and dotted black lines represent the lower and upper delay boundaries of the stability region. These boundaries are numerically obtained by DDE-BIFTOOL [41], a bifurcation analysis tool for time-delayed systems. We see that

---

[4]Amplitude$(x) := \max_{t\in[2900,3000]} \{x(t)\} - \min_{t\in[2900,3000]} \{x(t)\}$.
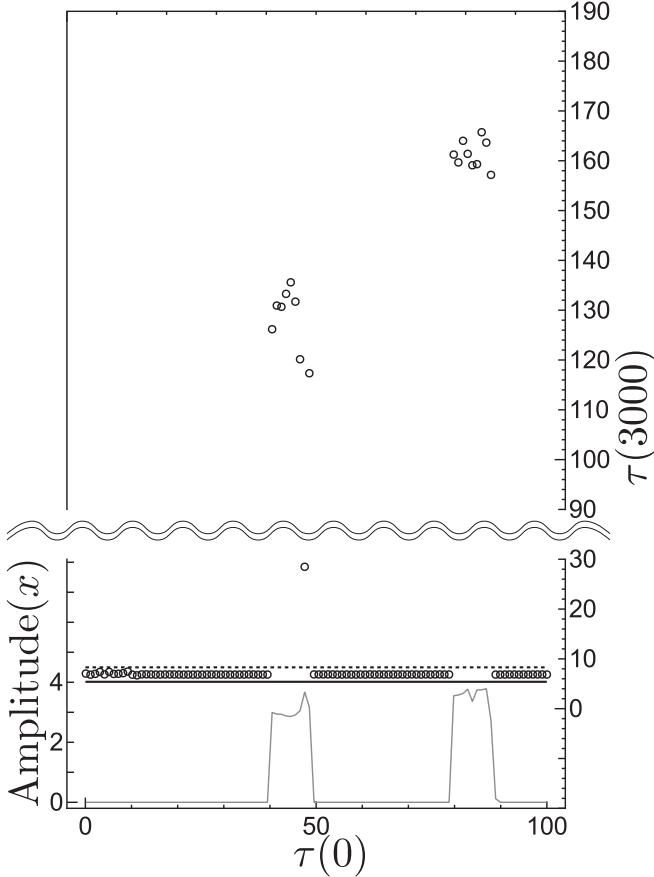
FIG. 7. Influence of initial delay time $\tau(0)$ on adaptive tuning (2) for FHN model (13). The horizontal axis represents the initial delay time $\tau(0)$. The solid gray line represents the amplitudes of $x(t)$ for $t \in [2900, 3000]$. The solid black line and dotted black line represent the lower and upper delay boundaries for the stability region. The open circles indicate the delay time $\tau(t)$ at $t = 3000$.

$\tau(t)$ at $t = 3000$, plotted as the open circles, lies between the lower and upper delay boundaries if stabilization is achieved (i.e., the amplitudes of x are zeros). Stabilization is successfully achieved for all $\tau(0)$ smaller than the period 39.5 of the stable limit cycle without control. However, for 30% of $\tau(0) \in (39.5, 100]$, tuning rule (2) fails to stabilize the USS: $\tau(t)$ becomes significantly large, and the amplitudes of x are around 3.3. It can be seen that the success or failure of the stabilization depends on whether $\tau(0)$ is smaller or larger than the period of the stable limit cycle without control. This result agrees with that for the SL oscillator in Fig. 5.

B. Lorenz system

Let us consider the Lorenz system [40], a well-known three-dimensional chaotic system, with DFC,

$$\dot{x}(t) = -10x(t) + 10y(t), \tag{14a}$$

$$\dot{y}(t) = 28x(t) - y(t) - x(t)z(t) - k\{y(t) - y[t - \tau(t)]\},$$
$$\tag{14b}$$

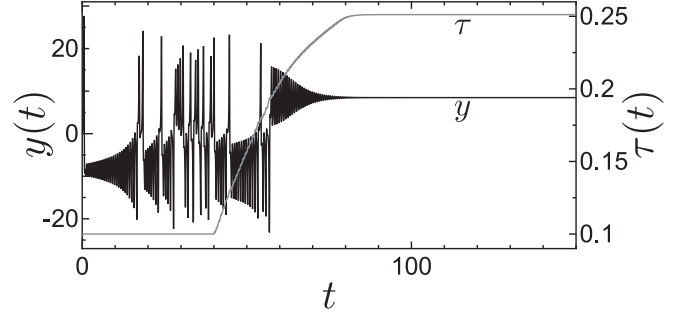$$\dot{z}(t) = -\tfrac{8}{3}z(t) + x(t)y(t), \tag{14c}$$

FIG. 8. Time series of state variable $y(t)$ and delay time $\tau(t)$ in Lorenz system (14) with adaptive tuning (2) for $k = 0.4$, $\beta = 0.01$, and $\gamma = 100$.

where $x(t), y(t), z(t) \in \mathbb{R}$ are the state variables. The Lorenz system has a saddle $(x, y, z) = (0, 0, 0)$ and two unstable foci $(x, y, z) = (\pm 8.4853, \pm 8.4853, 27)$. In general, DFC never stabilizes the saddle due to the odd-number property for USSs [12,13] (see Appendix C for more details); thus, we concentrate on the foci. The adaptive tuning (2) uses $y(t)$ instead of $z(t)$. The parameters are set to $k = 0.4$, $\beta = 0.01$, and $\gamma = 100$. Figure 8 shows the time series of $y(t)$ and $\tau(t)$ with $(x(0), y(0), z(0), u(0), \tau(0)) = (0.1, 0, 0, 0, 0.1)$, where DFC with the tuning starts at $t = 40$. We see that $y(t)$ converges on one of the foci adaptively.

We numerically investigate the influence of $\tau(0) \in [0.1, 20]$ on the performance of tuning (2). The parameters and other initial conditions are the same as for Fig. 8. In Fig. 9, the amplitudes of $y(t)$ for $t \in [2900, 3000]$ (solid gray line) and $\tau(t)$ at $t = 3000$ (open circles) are plotted against $\tau(0) \in [0.1, 20]$. We can see that there are several stability regions with lower and upper delay boundaries (i.e., the solid and dotted black lines). For all $\tau(0) \in [0.1, 14)$, $\tau(t)$ adaptively moves into the stability region near its initial condition $\tau(0)$, and the amplitude of $y(t)$ then converges to zero. For example, with $\tau(0) = 3.52$, 6.93, and 10.55, $\tau(3000)$ reaches 3.39, 6.38, and 10.13, respectively. For $\tau(0) \in [14, 20]$, stabilization cannot be achieved due to a lack of stability regions around $\tau(0)$. It can be concluded from Fig. 9 that $\tau(0)$ should be small to achieve stabilization. Furthermore, we see that the adaptive tuning works well even for a chaotic system.

C. Comparison to adaptive techniques [29,30]

To the best of our knowledge, adaptive tuning of the delay time for stabilizing only USSs has not yet been proposed. However, there are a few adaptive tuning rules for delay time that have the potential for stabilizing USSs [29,30]. This subsection discusses two previous studies [29,30] and compares the control performance of tuning rule (2) to that of the previous studies based on numerical simulations. The parameters (λ, ω, k), the initial amplitude $r(0)$, the tuning start time, and the symbols of Fig. 5 are also considered.

Nakajima *et al.* proposed an adaptive tuning rule for stabilizing UPOs [29], but not USSs. However, USSs can be unintentionally stabilized by this rule [29]. Figures 10(a)–10(c) show the trajectories of SL oscillator (11) with tuning for the three cases $b = 0$, $b < 0$, and $b > 0$, respectively. The circles represent the convergence points on periodic
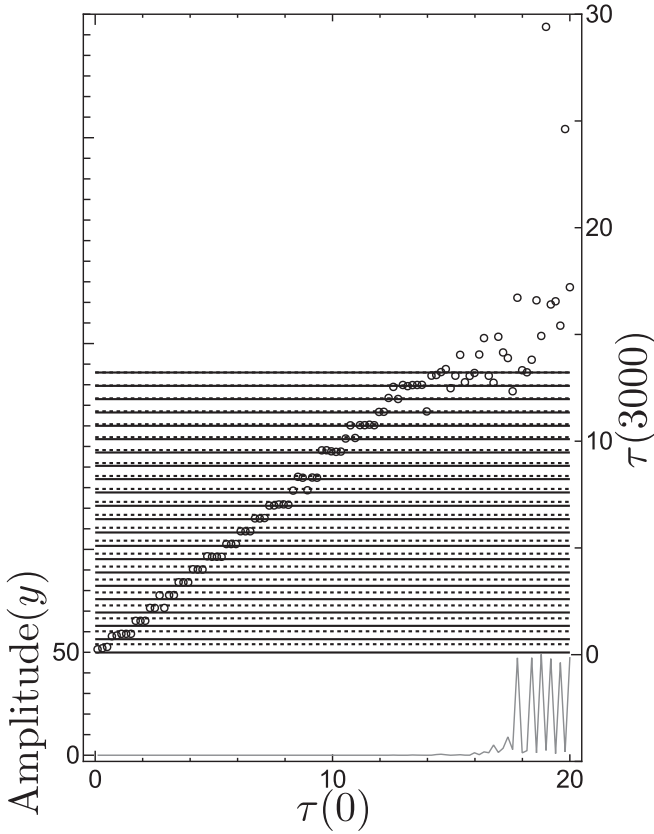
FIG. 9. Influence of initial delay time $\tau(0)$ on adaptive tuning (2) in Lorenz system (14). The lines and symbols are the same as those in Fig. 7.

orbits. As can be seen, the trajectories starting from initial delays (i.e., black dots) fall down to the stable r^* [i.e., cyan (light gray) dots] and follow the stable r^* upwards. As a result, they finally converge on periodic orbits (i.e., circles). Since the tuning rule [29] is intended for stabilizing UPOs, the trajectories behave to avoid USSs. As an exception, the trajectory starting from $\tau(0) = 1.05$ (i.e., middle black dot) shown in Fig. 10(a) falls down to the stable steady state (i.e., the square) without crossing the stable r^*. This fact suggests that the tuning rule [29] can stabilize USSs only when the initial delay $\tau(0)$ is within the stability region. It can be concluded that the tuning rule [29] performs well in stabilizing UPOs but does not perform for stabilizing USSs.

Lin *et al.* proposed an adaptive tuning rule which can stabilize both UPOs and USSs [30]. The tuning rule is described as

$$\dot{\tau} = -r_1\{x[t - \tau(t)] - x(t)\}, \tag{15a}$$

$$\dot{k} = r_2\{x[t - \tau(t)] - x(t)\}^2, \tag{15b}$$

where Eqs. (15a) and (15b) are the rules for the delay time and the feedback gain, respectively. To facilitate a fair comparison to the rules of Eq. (2) and of the study of Ref. [29], we do not use Eq. (15b) and we fix $k = 0.6$. Figures 11(a)–11(c) show the trajectories of SL oscillator (11) with this tuning rule. We now focus on the case $b = 0$ [see Fig. 11(a)]. The trajectory starting from $\tau(0) = 0.1$ (i.e., left black dot) converges on the steady state (i.e., square), thus successfully achieving stabilization of the USS. In contrast, the other trajectories converge
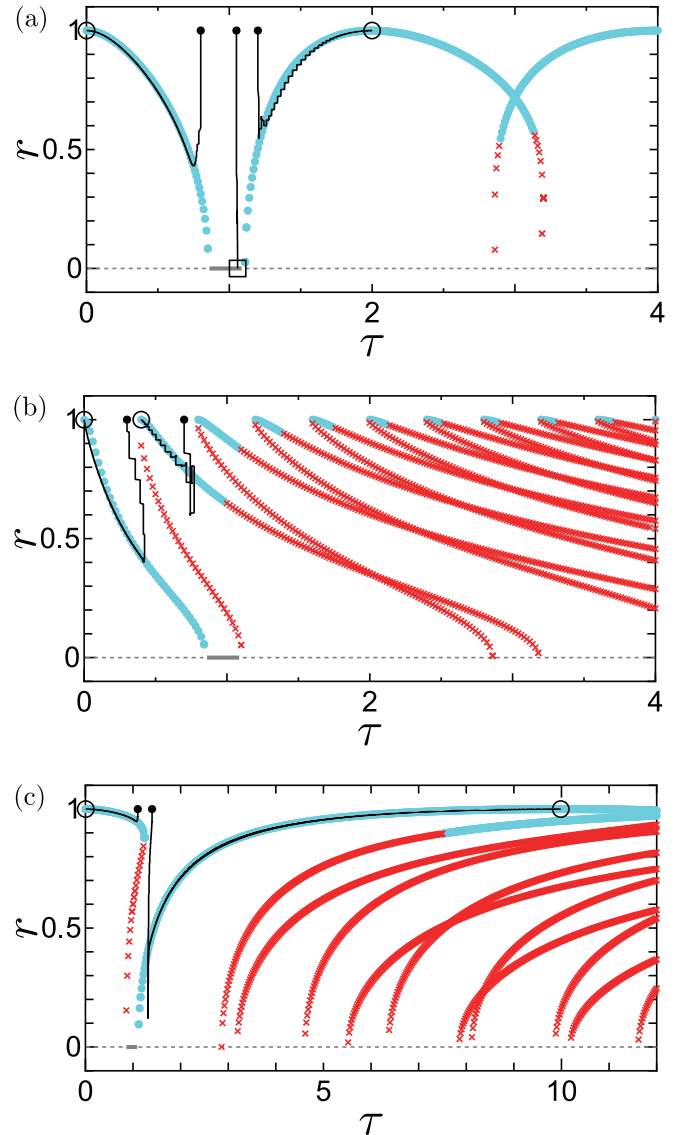

FIG. 10. Trajectories of SL oscillator (11) with adaptive tuning proposed in Ref. [29] for (a) $b = 0$, (b) $b = -4\pi$, and (c) $b = 0.8\pi$. The parameters (λ, ω, k) and the symbols are the same as in Fig. 5. The circles represent the convergence points on periodic orbits. We set $\eta = 0.01$ in the rule of Ref. [29]. The initial delay times are set to (a) $\tau(0) \in \{0.8\ 1.05,\ 1.2\}$, (b) $\tau(0) \in \{0.3,\ 0.7\}$, and (c) $\tau(0) \in \{1.1,\ 1.4\}$.

on the periodic orbits (i.e., circles), i.e. the stabilization of the USS fails. Figures 11(a)–11(c) show that the trajectories starting from the initial delays (i.e., black dots) always move toward the right with small oscillatory behavior. Then, the trajectories stop at the steady states with $r^* = 0$ or the periodic orbits with $r^* = 1$, since these states and orbits satisfy $x(t) = x[t - \tau(t)]$. These findings indicate that the successful stabilization of USSs strongly depends on $\tau(0)$.

Now we compare rule (2) to those of the two studies with regard to the stabilization of USSs. We focus on the set of initial delays which achieve stabilization of USSs. We notice that the set for rule (2) is larger than for the two studies. It should be emphasized that for $b = 0.8\pi > 0$, although the trajectories for the two studies [see Figs. 10(c) and 11(c)]
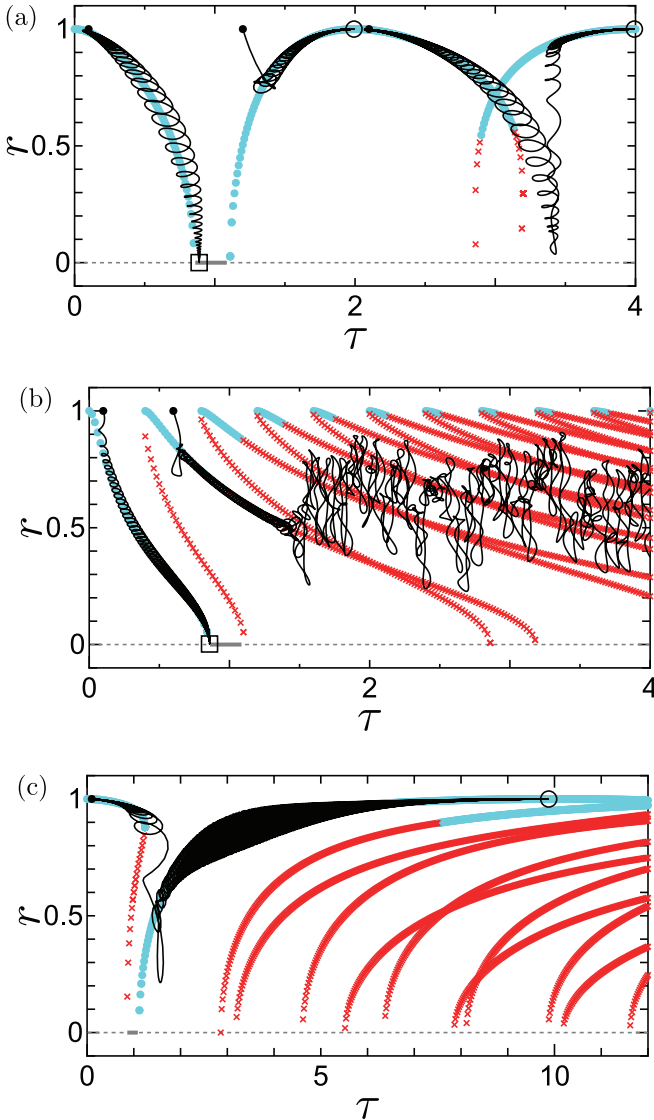
FIG. 11. Trajectories of SL oscillator (11) with adaptive tuning proposed in Ref. [30] for (a) $b = 0$, (b) $b = -4\pi$, and (c) $b = 0.8\pi$. The parameters (λ, ω, k) and the symbols are the same as in Fig. 10. We set $r_1 = 0.3$ and $r_2 = 0$ in the rule of Ref. [30]. The initial delay times are set to (a) $\tau(0) \in \{0.1\ 1.2,\ 2.1\}$, (b) $\tau(0) \in \{0.1,\ 0.6\}$, and (c) $\tau(0) = 0.1$.

cannot converge on a steady state, the trajectories for rule (2) [see Fig. 5(c)] successfully converge on USS. It may be said that rule (2) shows the best performance for the stabilization of USSs.

VI. DISCUSSIONS

It has been widely accepted that the stabilization of USSs is a powerful solution for eliminating harmful oscillatory behavior in real applications; hence, several control methods for stabilizing USSs with noninvasive properties have been proposed. This section overviews these methods, which can be categorized as those using DFC and those not using DFC.

We see that, to achieve stabilization of USSs with DFC, the delay time has to be carefully chosen from the stability ranges. It was reported that the ranges can be expanded by adding some modifications to DFC. Socolar, Sukow, and Gauthier reported an improved DFC, known as extended DFC, in which many previous states are used to generate control signals [42–44]. Ahlborn and Parlitz applied different independent delay times to DFC [45–47]. Gjurchinovski *et al.* periodically varied the delay time of DFC at high frequencies [48,49]. Although these modifications are useful for expanding the stability range of delay, it is necessary to add a feedback loop, to use an additional delay, or to continue to vary the delay time. Moreover, to design the delay time for these modifications, a knowledge of USSs is required. In contrast, DFC with adaptive tuning (2) does not need such additions, usage, and continuation, and also does not require knowledge of USSs.

Let us briefly overview the control methods other than DFC. It was reported that a derivative control method can be used to stabilize USSs [50–53]. The method is highly sensitive to high-frequency noise; thus, alternative methods resistant to noise that employ a high-pass filter [54] or a low-pass filter [55,56],[5] were proposed. Note that, to design the feedback gain of such filters, a knowledge of USSs is required. We are aware of two techniques using filters which can avoid requiring knowledge of USSs: setting the gain sufficiently high [57] and adaptively tuning the gain [58–61]. Although these techniques are useful for stabilizing unknown USSs, the feedback gain for these techniques tends to be very high. For practical implementations, such a high gain makes the control signals large, which is undesirable for real situations. In contrast, DFC with adaptive tuning (2) does not require a high gain. In addition, for real applications where the implementation of filters is difficult, such as metal cutting processes [62], DFC with adaptive tuning (2) is a reasonable solution to eliminate harmful oscillations.

VII. CONCLUSION

The present paper proposes an adaptive tuning rule for the delay time that stabilizes only USSs based on the gradient descent method. It was shown that the delay time near the stability region is automatically tuned to fall into the stability region and to remain there. The numerical results for a Stuart–Landau oscillator reveal that the stabilization with the tuning rule depends on the structure of stable periodic orbits, the type of bifurcation, and the initial delay. We found that for small initial delays, the stabilization is achieved robustly for bifurcation-type structures. It was numerically demonstrated that the tuning rule shows good performance even for the FitzHugh–Nagumo model and Lorenz system. Furthermore, we showed that, from the viewpoint of the stabilization of USSs, the tuning rule works better than other rules for stabilizing USSs.

———————

[5]The methods with a low-pass filter can stabilize various types of USSs, if the stability of the filter is set based on its type [55].
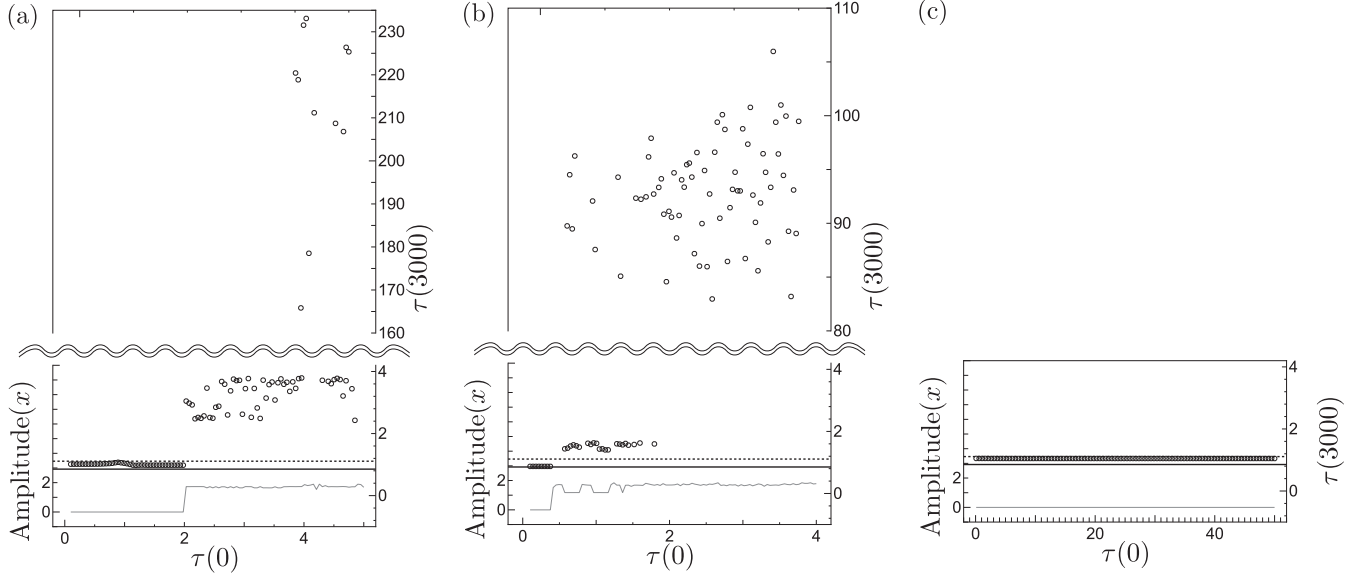
FIG. 12. Influence of initial delay time $\tau(0)$ on adaptive tuning (2) for SL oscillator (11). The lines and symbols are the same as those in Figs. 7 and 9: (a) $b = 0$ (period 2), (b) $b = -4\pi$ (period 0.4), and (c) $b = 0.8\pi$ (period 10).

APPENDIX A: DETAILS FOR PROPERTIES 1 AND 2

This Appendix provides details regarding Properties 1 and 2 in Sec. III C. It should be noted that, since the linear system (4) with rule (2) has a state-dependent time delay, its stability cannot be analyzed based on characteristic functions. However, since $\tau(t)$ varies sufficiently slowly due to the small value of β, this Appendix discusses the behavior of $\tau(t)$ on the assumption that $z(t)$ behaves in almost the same manner as for conventional DFC. It must be emphasized that here we provide a rough estimation of the behavior without rigorous proof. First, we consider Property 1. Such approximate behavior is governed by characteristic roots $\Lambda = p \pm iq$, as shown in Fig. 3. Thus, the polar representation $z(t) = r(t) \exp\{i\theta(t)\}$ allows us to make the approximation $z(t - \tau) \approx r(t) \exp[-p\tau + i\{-q\tau + \theta(t)\}]$. As a result, function (8) can be expressed as

$$\Delta(t, \tau) = -\{r^2(t) + r^2(t)e^{-2p\tau} - 2r^2(t)e^{-p\tau}\cos q\tau\}. \quad (A1)$$

Therefore, we have

$$\frac{d\Delta(t, \tau)}{d\tau} = 2r^2(t)e^{-p\tau}\{pe^{-p\tau} - p\cos q\tau - q\sin q\tau\}. \quad (A2)$$

It is obvious that $p = 0$ holds if τ is on the stability boundary (7). Hence, in the vicinity of the boundary, we have

$$\frac{d\Delta(t, \tau)}{d\tau} \approx -2r^2(t)q\sin q\tau. \quad (A3)$$

Here, if τ is on the boundary (7), then the imaginary parts of the characteristic roots [15] are given by

$$q = \begin{cases} \omega - \sqrt{(2k - \lambda)\lambda} & \text{for } \tau = \tau_{1,n}, \\ \omega + \sqrt{(2k - \lambda)\lambda} & \text{for } \tau = \tau_{2,n}. \end{cases} \quad (A4)$$

By substituting Eqs. (7) and (A4) into Eq. (A3), we see that the sign of $d\Delta(t, \tau)/d\tau$ is negative for $\tau = \tau_{1,n}$ and positive for $\tau = \tau_{2,n}$. From Eqs. (2) and (10), the sign of $\dot{\tau}(t)$ is

written as

$$\begin{aligned} \dot{\tau}(t) &> 0 \quad \text{for } \tau = \tau_{1,n}, \\ \dot{\tau}(t) &< 0 \quad \text{for } \tau = \tau_{2,n}. \end{aligned} \quad (A5)$$

Second, we consider Property 2. Once $\tau(t)$ moves into the stability region, the state variables converge to $z(t) = z(t - \tau) = 0$ as $t \to +\infty$. Thus, we have $\dot{\tau} \to 0$ as $t \to +\infty$ due to rule (2).

APPENDIX B: INFLUENCE OF $\tau(0)$ FOR SL OSCILLATOR

This Appendix shows the influence of the initial delay $\tau(0)$ on the performance of adaptive tuning (2) for SL oscillator (11) in the same manner as in Figs. 7 and 9. The parameters and other initial conditions are the same as for Fig. 5. The amplitudes of $x(t) = \text{Re}[z(t)]$ and the delay $\tau(t)$ at $t = 3000$ are plotted against $\tau(0) \in [0.1, 5]$ for $b = 0$, $\tau(0) \in [0.1, 4]$ for -4π, and $\tau(0) \in [0.1, 50]$ for 0.8π in Figs. 12(a)–12(c), respectively. As can be seen, for any $b \in \{0, -4\pi, 0.8\pi\}$, the stabilization is successfully achieved for all $\tau(0)$ smaller than the period of the stable limit cycle without control, where the period is 2 for $b = 0$, 0.4 for $b = -4\pi$, and 10 for $b = 0.8\pi$.

APPENDIX C: ODD-NUMBER PROPERTY FOR USSS

The odd-number property for USSs is known as follows: If the Jacobian matrix at a USS has an odd number of real positive eigenvalues, then the USS cannot be stabilized by conventional DFC for any feedback gain and any delay time [12,13]. As the matrix at the saddle has one positive real eigenvalue, the property guarantees that the saddle cannot be stabilized by conventional DFC. This fact shows that, even with adaptive tuning (2), the saddle cannot be stabilized, since DFC with tuning at USSs performs as conventional DFC owing to Property 2.

It is well known that the odd-number property for UPOs has been refuted [63,64] (see review article [65] and

references therein). However, it was reported in Ref. [66] that the property for USSs is still valid for the form of DFC used in the present paper, as described in Eq. (14).

[1] E. Schöll and H. G. Schuster, eds., *Handbook of Chaos Control* (Wiley, Weinheim, 2007).

[2] K. Pyragas, Phys. Lett. A **170**, 421 (1992).

[3] W. Just, T. Bernard, M. Ostheimer, E. Reibold, and H. Benner, Phys. Rev. Lett. **78**, 203 (1997).

[4] K. Pyragas, Phys. Rev. E **66**, 026207 (2002).

[5] K. Pyragas, V. Pyragas, and H. Benner, Phys. Rev. E **70**, 056222 (2004).

[6] V. Flunkert and E. Schöll, Phys. Rev. E **84**, 016214 (2011).

[7] V. Pyragas and K. Pyragas, Commun. Nonlinear Sci. Numer. Simul. **73**, 338 (2019).

[8] A. Cetinkaya and T. Hayakawa, IEEE Trans. Autom. Control **64**, 3748 (2019).

[9] Y.-G. Zheng and M.-H. Liu, J. Franklin Inst. **359**, 8484 (2022).

[10] Z. Zhang, J. P. Chávez, J. Sieber, and Y. Liu, Int. J. Non-Linear Mech. **152**, 104390 (2023).

[11] M. Watanabe and K. Sakai, Sci. Rep. **13**, 10695 (2023).

[12] H. Kokame, K. Hirata, K. Konishi, and T. Mori, IEEE Trans. Autom. Control **46**, 1908 (2001).

[13] H. Kokame, K. Hirata, K. Konishi, and T. Mori, Int. J. Control **74**, 537 (2001).

[14] K. Pyragas, V. Pyragas, I. Z. Kiss, and J. L. Hudson, Phys. Rev. Lett. **89**, 244103 (2002).

[15] P. Hövel and E. Schöll, Phys. Rev. E **72**, 046203 (2005).

[16] C.-U. Choe, R.-S. Kim, P. Hövel, and E. Schöll, Int. J. Dyn. Control **4**, 123 (2016).

[17] S. Yanchuk, M. Wolfrum, P. Hövel, and E. Schöll, Phys. Rev. E **74**, 026201 (2006).

[18] H. Huijberts, W. Michiels, and H. Nijmeijer, SIAM J. Appl. Dyn. Syst. **8**, 1 (2009).

[19] J. Čermák and L. Nechvátal, Physica D **404**, 132339 (2020).

[20] S. K. Gupta, J. Wang, and O. R. Barry, Nonlinear Dyn. **101**, 439 (2020).

[21] B. Rezaie and M.-R. J. Motlagh, Nonlinear Dyn. **64**, 167 (2011).

[22] J. Lehnert, P. Hövel, V. Flunkert, P. Yu. Guzenko, A. L. Fradkov, and E. Schöll, Chaos **21**, 043111 (2011).

[23] V. Pyragas and K. Pyragas, Eur. Phys. J. B **86**, 306 (2013).

[24] A. Selivanov, J. Lehnert, A. Fradkov, and E. Schöll, Phys. Rev. E **91**, 012906 (2015).

[25] A. Kittel, J. Parisi, and K. Pyragas, Phys. Lett. A **198**, 433 (1995).

[26] G. Chen and X. Yu, IEEE Trans. Circuits Syst. I **46**, 767 (1999).

[27] X. Yu, IEEE Trans. Circuits Syst. I **46**, 1408 (1999).

[28] V. Pyragas and K. Pyragas, Phys. Lett. A **375**, 3866 (2011).

[29] H. Nakajima, H. Ito, and Y. Ueda, IEICE Trans. Fundam. Electr. Commun. Comput. Sci. **E80-A**, 1554 (1997).

[30] W. Lin, H. Ma, J. Feng, and G. Chen, Phys. Rev. E **82**, 046214 (2010).

[31] Y. M. Chen, Q. X. Liu, and J. K. Liu, Acta Mech. Sin. **36**, 918 (2020).

[32] J. Munoa, X. Beudaert, Z. Dombovari, Y. Altintas, E. Budak, C. Brecher, and G. Stepan, CIRP Ann. **65**, 785 (2016).

[33] A. P. Dowling and A. S. Morgans, Annu. Rev. Fluid Mech. **37**, 151 (2005).

[34] S. Singh, A. R. Gautam, and D. Fulwani, Renew. Sustain. Energy Rev. **72**, 407 (2017).

[35] S. H. Strogatz, D. M. Abrams, A. McRobie, B. Eckhardt, and E. Ott, Nature **438**, 43 (2005).

[36] R. C. Hinz, P. Hövel, and E. Schöll, Chaos **21**, 023114 (2011).

[37] K. Yoshida, K. Konishi, and N. Hara, Nonlinear Dyn. **106**, 2363 (2021).

[38] R. FitzHugh, Biophys. J. **1**, 445 (1961).

[39] J. Nagumo, S. Arimoto, and S. Yoshizawa, Proc. IRE **50**, 2061 (1962).

[40] E. N. Lorenz, J. Atmos. Sci. **20**, 130 (1963).

[41] K. Engelborghs, T. Luzyanina, and D. Roose, ACM Trans. Math. Softw. **28**, 1 (2002).

[42] J. E. S. Socolar, D. W. Sukow, and D. J. Gauthier, Phys. Rev. E **50**, 3245 (1994).

[43] T. Dahms, P. Hövel, and E. Schöll, Phys. Rev. E **76**, 056201 (2007).

[44] D. Costa, E. Pavlovskaia, and M. Wiercigroch, Chaos, Solitons Fractals **181**, 114570 (2024).

[45] A. Ahlborn and U. Parlitz, Phys. Rev. Lett. **93**, 264101 (2004).

[46] A. Ahlborn and U. Parlitz, Phys. Rev. E **72**, 016206 (2005).

[47] Z. Jiang and T. Zhang, Complexity **2020**, 4937569 (2020).

[48] A. Gjurchinovski, T. Jüngling, V. Urumov, and E. Schöll, Phys. Rev. E **88**, 032912 (2013).

[49] Q. Liu, J. Liu, and Y. Chen, Int. J. Nonlinear Mech. **126**, 103563 (2020).

[50] S. Bielawski, M. Bouazaoui, D. Derozier, and P. Glorieux, Phys. Rev. A **47**, 3276 (1993).

[51] P. Parmananda, M. A. Rhode, G. A. Johnson, R. W. Rollins, H. D. Dewald, and A. J. Markworth, Phys. Rev. E **49**, 5007 (1994).

[52] S. S. De Sarkar and S. Chakraborty, Int. J. Dyn. Control **6**, 827 (2018).

[53] K. M. Arthur and S. Y. Yoon, ISA Trans. **107**, 40 (2020).

[54] A. Chang, J. C. Bienfang, G. M. Hall, J. R. Gardner, and D. J. Gauthier, Chaos **8**, 782 (1998).

[55] K. Pyragas, V. Pyragas, I. Z. Kiss, and J. L. Hudson, Phys. Rev. E **70**, 026215 (2004).

[56] T. Pyragienė and K. Pyragas, Phys. Lett. A **492**, 129232 (2023).

[57] H. Ma, D. W. C. Ho, Y.-C. Lai, and W. Lin, Phys. Rev. E **92**, 042902 (2015).

[58] D. J. Braun, Phys. Rev. E **78**, 016213 (2008).

[59] W. Lin, Phys. Rev. E **81**, 038201 (2010).

[60] D. J. Braun, Phys. Rev. E **81**, 038202 (2010).

[61] B. C. Rout, D. K. Lal, and A. Barisal, Cogent Eng. **4**, 1362804 (2017).

[62] T. Insperger, G. Stépán, and J. Turi, Nonlinear Dyn. **47**, 275 (2006).

[63] B. Fiedler, V. Flunkert, M. Georgi, P. Hövel, and E. Schöll, Phys. Rev. Lett. **98**, 114101 (2007).

[64] W. Just, B. Fiedler, M. Georgi, V. Flunkert, P. Hövel, and E. Schöll, Phys. Rev. E **76**, 026210 (2007).

[65] N. Kuznetsov, G. Leonov, and M. Shumafov, IFAC-PapersOnLine **48**, 706 (2015).

[66] G. A. Leonov, M. M. Shumafov, and N. V. Kuznetsov, Differ. Equ. **52**, 1707 (2016).